ISSN 0965-5425, Computational Mathematics and Mathematical Physics, 2021, Vol. 61, No. 1, pp. 1–16. © Pleiades Publishing, Ltd., 2021.
Russian Text © The Author(s), 2021, published in Zhurnal Vychislitel'noi Matematiki i Matematicheskoi Fiziki, 2021, Vol. 61, No. 1, pp. 3–19.

GENERAL NUMERICAL METHODS

EBR Schemes with Curvilinear Reconstructions of Variables in the Near-Wall Region

A. P. Duben[a], T. K. Kozubskaya[a], P. V. Rodionov[a,*], and V. O. Tsvetkova[a]

[a] *Federal Research Center Keldysh Institute of Applied Mathematics, Russian Academy of Sciences, Moscow, 125047 Russia*

**e-mail: rodionov.cs@gmail.com*

Received May 13, 2020; revised June 5, 2020; accepted September 18, 2020

Abstract—Higher accuracy vertex-centered EBR schemes for gasdynamic simulations on unstructured meshes are developed. The schemes are equipped with the option of using a quasi-one-dimensional curvilinear stencil for reconstructing variables on a structured or semi-structured anisotropic mesh in the near-wall region. In the two-dimensional case, the use of curvilinear reconstruction leads to the natural transformation of an EBR scheme into a structured mesh finite-volume method. In the three-dimensional case, an original algorithm for finding stencil points and corresponding metric coefficients is developed to implement curvilinear reconstructions of variables in prismatic layers. The effect exerted by curvilinear reconstructions used in EBR schemes as applied to external flow problems is demonstrated on the well-known test problem of the flow around the NACA0012 airfoil considered in two- and three-dimensional formulations. The new algorithm is validated by comparing the solution with experimental data and numerical results of other authors. The use of curvilinear reconstructions in EBR schemes enhances the stability of the method and improves the accuracy of the numerical results.

Keywords: EBR scheme, quasi-one-dimensional reconstruction, curvilinear stencil, semi-structured mesh, boundary layer, external flow problem

DOI: 10.1134/S0965542520120039

INTRODUCTION

The correct simulation of external turbulent flows over bodies of arbitrary curvilinear geometry depends fundamentally on the accuracy of reproducing the arising boundary layers. For this purpose, a sufficiently detailed grid resolution in the wall-normal direction is required under mesh refinement toward the body surface. In the longitudinal direction, the values of variables vary more smoothly, so the mesh size in this direction can be rather large. This feature of boundary-layer turbulent flows is best captured by layers of anisotropic meshes surrounding the body. In the case of unstructured meshes, closed boundary layers or individual layered areas form structured or semi-structured subdomains. Over extended segments of the body, the flow is directed along the curvilinear surfaces separating the layers (or the lines in the two-dimensional case).

The accuracy of simulation can be improved substantially when the numerical method takes into account the features of the near-wall flow and the mesh structure in the near-wall region. This is especially true of methods using spatial approximations of variables on extended stencils.

In this paper, we consider algorithms based on vertex-centered edge-based reconstruction (EBR) schemes for unstructured meshes [1]. These schemes have higher accuracy, which is ensured by the reconstruction of flux variables on extended edge-based stencils. Moreover, these schemes are more efficient, which is ensured by the quasi-one-dimensional nature of this approach. Initially developed for arbitrary tetrahedral meshes, EBR schemes can be generalized to hybrid unstructured meshes [2]. However, on curvilinear structured meshes with a high degree of mesh element anisotropy, the use of EBR schemes in their original formulation involving *rectilinear* reconstruction (i.e., reconstruction on rectilinear stencils) might lead to degraded numerical accuracy and instability development. In this paper, we examine the causes of these negative phenomena. To overcome the arising difficulties, we use curvilinear stencils for reconstructions of variables (in other words, *curvilinear* reconstructions), which take into account the

mesh structure in the near-wall region. A similar approach for the flux correction method was implemented in [3, 4].

The goal of this work is to implement the technique of curvilinear reconstructions in EBR schemes in the two-dimensional case and, most importantly, to develop a new efficient algorithm for curvilinear reconstruction on semi-structured meshes in the three-dimensional case. The effect of using curvilinear reconstruction is demonstrated by numerically solving a classical validation problem, namely, the flow over the NACA0012 airfoil [5] in two- and three-dimensional formulations.

1. MATHEMATICAL MODEL

Consider the compressible Navier–Stokes equations

$$\frac{\partial \mathbf{Q}}{\partial t} + \nabla \cdot F(\mathbf{Q}) = \nabla \cdot F_v(\mathbf{Q}, \nabla \mathbf{Q}), \tag{1}$$

written in conservative variables, where

$$\mathbf{Q} = \begin{pmatrix} \rho \\ \rho \mathbf{u} \\ E \end{pmatrix}, \quad F = \begin{pmatrix} \rho \mathbf{u} \\ \rho \mathbf{u}\mathbf{u} + pI \\ (E + p)\mathbf{u} \end{pmatrix}, \quad F_v = \begin{pmatrix} 0 \\ \sigma \\ \sigma \mathbf{u} - \mathbf{q} \end{pmatrix}.$$

Here, ρ is the density, $\mathbf{u}$ is the velocity, p is the pressure, E is the total energy, and I is the identity matrix. The stress tensor and the heat flux are defined as $\sigma = \mu(\nabla \mathbf{u} + (\nabla \mathbf{u})^{\mathrm{T}} - (2/3)(\nabla \cdot \mathbf{u})I)$ and $\boldsymbol{q} = -k\nabla T$, respectively, where μ is the dynamic viscosity, k is the thermal conductivity, and T is the temperature. The dynamic viscosity will be determined according to Sutherland's law.

In this paper, we also use the Navier–Stokes equations (1) averaged according to Reynolds, i.e., the Reynolds-averaged Navier–Stokes (RANS). The Reynolds stress tensor involved in the RANS system is closed using the Spalart–Allmaras (SA) linear turbulence model [6] written with respect to the modified eddy viscosity. In this case, the general form of the viscous fluxes F_v remains unchanged up to the eddy viscosity, which is added to the dynamic viscosity.

2. NUMERICAL METHOD BASED ON THE ORIGINAL EBR SCHEME

To solve system (1) numerically on an arbitrary mesh, we construct a scheme with variables determined at mesh nodes. In what follows, such schemes are referred to as *vertex-centered*. Around each node, we construct median cells, for which, according to the finite-volume approach, difference analogues of conservation laws are formulated. Examples of median cells for a two-dimensional mesh are shown in Fig. 1. The grid function $\mathbf{Q}_i$ is defined as the integral mean of the function $\mathbf{Q}$ over the cell constructed around the node i. By using the Ostrogradsky–Gauss formula, system (1) is rewritten in vector-matrix form as

$$V_i \frac{d\mathbf{Q}_i}{dt} + \sum_{j \in N_1(i)} \mathbf{F}_{ij} s_{ij} = F_{i,v},$$

where V_i is the volume of the cell corresponding to node i, $\mathbf{F}_{ij}$ is the integral mean of the function $F\mathbf{n}$ over the cell face separating nodes i and j, s_{ij} is the area of this cell face, $\mathbf{n}$ is the unit normal vector, $N_1(i)$ is the set of first-order neighbor for node i, and $F_{i,v}$ is an integral function of the viscous flux F_v on the cell corresponding to node i. The convective fluxes $\mathbf{F}_{ij}$ are computed using the Roe method for the approximate solution of the Riemann problem:

$$\mathbf{F}_{ij} = \frac{1}{2}(\mathbf{F}_{ij}^R + \mathbf{F}_{ij}^L) - \frac{1}{2}|A_{ij}|(\mathbf{Q}_{ij}^R - \mathbf{Q}_{ij}^L).$$

The values $\mathbf{Q}_{ij}^{L/R}$ to the left and right of the interface are determined using quasi-one-dimensional reconstructions $R_{ij}^{L/R}\{\mathbf{Q}\}$ defined on stencils whose points belong to the straight line containing the edge ij. The values of the fluxes $\mathbf{F}_{ij}^{L/R}$ are set equal to $F(R_{ij}^{L/R}\{\mathbf{Q}\})\mathbf{n}_{ij}$ or $R_{ij}^{L/R}\{F\mathbf{n}_{ij}\}$ depending on the chosen type of reconstructions [7]. Here, $\mathbf{n}_{ij}$ is the integral mean of the vector $\mathbf{n}$ over the common face between the cells

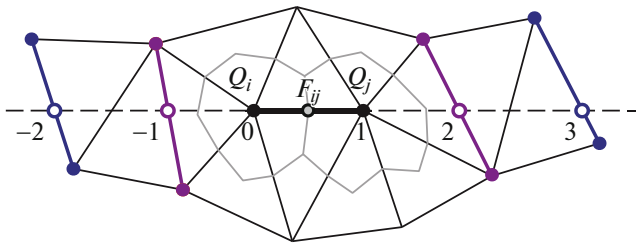

Fig. 1. Stencil of the EBR5 scheme for edge ij on a triangular unstructured mesh.

corresponding to nodes i and j, $|A_{ij}| = \left|\frac{dF\mathbf{n}}{d\mathbf{Q}}(\mathbf{Q}_{ij})\right| = S_{ij}|\Lambda_{ij}|S_{ij}^{-1}$, $\mathbf{Q}_{ij}$ is the Roe average computed over the values $\mathbf{Q}_{ij}^{L/R}$, and S_{ij} and Λ_{ij} are the matrices of eigenvectors and eigenvalues of the operator $\frac{dF\mathbf{n}}{d\mathbf{Q}}$ corresponding to $\mathbf{Q}_{ij}$. The scheme thus designed involves edge-based reconstructions of variables and, in a broad sense, belongs to the class of EBR schemes. In a narrower sense, according to [1], EBR schemes make use of reconstructions that, on translation-invariant meshes (i.e., ones mapped into itself under the translation through the vector of any mesh edge) transform the given method in a high order finite-difference scheme. Moreover, a scheme of this family is called an EBR n scheme if, in the linear case, its order on translation-invariant meshed is equal to n.

Below, the method for constructing quasi-one-dimensional reconstructions used in the original formulation of EBR schemes [1] is described for the EBR5 scheme in the two-dimensional formulation (Fig. 1). Suppose that we need to reconstruct the value of a function $\mathbf{Q}$ at the midpoint of an edge ij. For each node of edge ij, we construct the sets of its first- and second-order topological neighbors. The intersection point of the ray ji with the set of faces all of whose nodes are second-order neighbors of node i is denoted by index -2, while the intersection point of this ray with the set of faces all of whose nodes are first-order neighbors of node i is denoted by index -1. If the former point is nonunique, the index -2 denotes the most distant point from node i. Similarly, for the ray ij and node j, we obtain points with indices 3 and 2, respectively. The values of $\mathbf{Q}$ at the points $\{-2, -1, 2, 3\}$ are determined using linear interpolation over the corresponding faces crossed by the ray. If nodes i and j are assigned indices 0 and 1, respectively, then the reconstruction operators for the function $\mathbf{Q}$ in terms of divided differences, namely,

$$\Delta_m^L\{\mathbf{Q}\} = \frac{\mathbf{Q}_{m+1} - \mathbf{Q}_m}{|\mathbf{r}_{m+1} - \mathbf{r}_m|}, \quad \Delta_m^R\{\mathbf{Q}\} = \Delta_{-m}^L\{\mathbf{Q}\}$$

can be written as

$$\begin{aligned} R_{ij}^L\{\mathbf{Q}\} &= \mathbf{Q}_i + \frac{|\mathbf{r}_i - \mathbf{r}_j|}{2}\sum_m \beta_m \Delta_m^L\{\mathbf{Q}\}, \\ R_{ij}^R\{\mathbf{Q}\} &= \mathbf{Q}_j - \frac{|\mathbf{r}_i - \mathbf{r}_j|}{2}\sum_m \beta_m \Delta_m^R\{\mathbf{Q}\}, \end{aligned} \tag{2}$$

where $\beta_{-2} = -1/15$, $\beta_{-1} = 11/30$, $\beta_0 = 4/5$, and $\beta_1 = -1/10$ [1]. In the EBR3 scheme, which has a shorter stencil, these coefficients are $\beta_{-2} = 0$, $\beta_{-1} = 1/3$, $\beta_0 = 2/3$, and $\beta_1 = 0$.

As was noted above, for linearized equations on translation-invariant meshes, the EBR5 and EBR3 schemes are theoretically fifth- and third-order accurate, respectively. In the arbitrary case, the numerical order of accuracy of the EBR3 and EBR5 schemes varies from 5/4 [8] to 3 [1] depending on the quality of the used unstructured mesh.

In the numerical method used to solve system (1) in this paper, convective fluxes are approximated by applying the EBR5 or EBR3 scheme. Viscous fluxes are approximated using the Galerkin method with piecewise linear basis functions (with a diagonalized mass matrix). Time stepping relies on a first-order implicit scheme with Newton linearization of the system of discrete equations. Within one Newton iteration, the system of linear algebraic equations is solved using the biconjugate gradient method with ILU0 preconditioner.

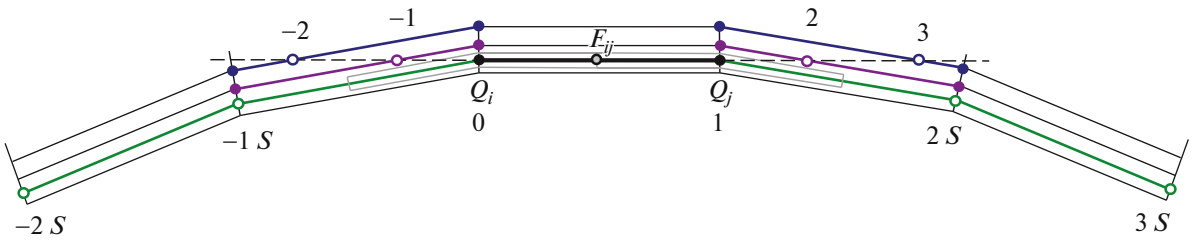

Fig. 2. Stencils of the EBR5 and EBR5 IJK/SS schemes for edge *ij* on an anisotropic structured mesh in the near-wall region.

3. EBR SCHEME WITH CURVILINEAR RECONSTRUCTIONS IN TWO-DIMENSIONAL STRUCTURED MESH DOMAINS WITHIN THE NEAR-WALL REGION

The EBR schemes described in Section 2 can be used, generally speaking, on arbitrary structured or unstructured meshes. However, as was noted in Section 2, the accuracy of these schemes is directly related to the quality of the mesh. For example, it has been shown that, on curvilinear meshes with a high degree of cell anisotropy, which are often used in boundary layer regions (Fig. 2) in aerodynamic flow problems, the standard reconstruction procedure on a *rectilinear* stencil based on the original formulation of EBR schemes may lead to a noticeable error of the numerical solution. The causes are as follows. First, a rectilinear reconstruction stencil leads to wide differences in the sizes of neighboring stencil steps, which may cause numerical instability. Second, since the geometry of the body is, generally speaking, curvilinear, the points of a rectilinear stencil might belong to different boundary-layer regions, which, in view of the high gradients of the flow, leads to increased variations in the functions values at these points and, hence, to a larger approximation error.

The indicated difficulties can be overcome to a large degree by replacing rectilinear reconstructions in EBR schemes with *curvilinear* ones (i.e., reconstructions on a curvilinear stencil), which naturally correspond to the mesh structure in the near-wall domain and to the properties of boundary-layer flow.

First, we consider curvilinear reconstructions in EBR schemes and methods for constructing corresponding curvilinear stencils in the case of two-dimensional aerodynamic flows, for which layers of structured meshes consisting of trapezoidal elements are usually used in boundary-layer regions (Fig. 2). Taking into account the structure of these meshes, the stencil points for a curvilinear reconstruction are specified not as the intersection points of the straight line *ij* with corresponding neighbor-order isosurfaces (points $\{-2, -1, 2, 3\}$ in Fig. 2), but rather as a certain number of nodes to the right and left of the nodes *i* and *j*, which are their structural neighbors (nodes $\{-2\text{ S}, -1\text{ S}, 2\text{ S}, 3\text{ S}\}$ in Fig. 2). It can be seen that this choice ensures an approximately equal step between the stencil points and a small variation in the values of the reconstructed function in the near-wall domain. The use of such a curvilinear stencil instead of a rectilinear one improves the stability of the resulting scheme and reduces the limitations on the admissible mesh geometry when the same formulas (2) are used for computing the reconstruction coefficients. It should also be noted that, in domains with sharp variations in mesh line directions, for example, near acute corners, curvilinear reconstructions might lose the indicated properties or even lead to increased errors and higher numerical instability. To eliminate this shortcoming, it is sufficient to specify a constraint on the maximum angle between the straight line *ij* and the directions of the curvilinear reconstruction stencil, under violation of which the algorithm is switched to the original EBR scheme.

The algorithm for the transition from curvilinear five-point reconstruction stencils of the EBR5 scheme in the near-wall region to standard rectilinear reconstructions away from this region can be conveniently organized step by step based on an analysis of the local mesh structure. For example, if there are no second-order structural neighbors, but there are corresponding first-order ones, it is possible to use a shortened curvilinear reconstruction stencil associated with the EBR3 scheme with passage to rectilinear reconstruction stencils only in the absence of first-order structural neighbors. Note that this approach to the construction of stencils in structured mesh subdomains is applicable along mesh lines in both tangential and normal directions to the body. The described method for choosing reconstruction was used in [9]. In what follows, the numerical results produced by two-dimensional EBR schemes that explicitly use *ijk-topology* in the construction of curvilinear stencils near the body are denoted by EBR IJK.

Let us formulate a somewhat different algorithm for constructing curvilinear reconstruction stencils that can easily be generalized to the three-dimensional case. According to this algorithm, each boundary mesh node is assigned a level of remoteness from the body surface defined as the minimum number of

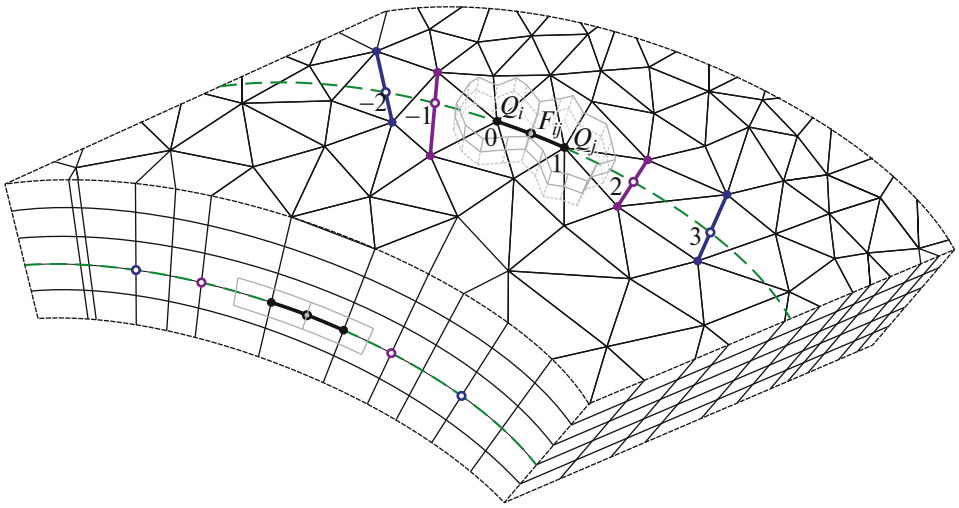

Fig. 3. Stencils of the EBR5 SS scheme for edge ij on a prismatic mesh in the near-wall region.

mesh edges joining this node to the surface. For nodes on the body surface, the level of remoteness is set to zero. If the edge ij lies on a contour line of the remoteness level, then the reconstruction stencil is made up of nodes of the required neighbor order having the same remoteness level. As before, formulas (2) for computing reconstruction coefficients remain unchanged. It is easy to see that the thus built reconstruction stencils along tangential mesh lines coincide with reconstruction stencils produced by automatic search for mesh structure. Edges that lie normally to the body and have vertices of different remoteness level are reconstructed according to the original EBR scheme, i.e., with the help of rectilinear stencils. Note that, due to the topology of the boundary structured mesh, the use of rectilinear or curvilinear reconstructions in the normal direction does not lead to a significant difference in the results.

4. EBR SCHEME WITH CURVILINEAR RECONSTRUCTIONS IN PRISMATIC MESH LAYERS WITHIN THE NEAR-WALL REGION

In practice, three-dimensional formulations in boundary-layer regions usually rely on layered hexahedral structured or prismatic semi-structured meshes. The latter are called *semi-structured* [10–13] because they are structured in the normal direction (a neighbor of each node in this direction is uniquely determined), but have no structure in tangential directions (Fig. 3). Reconstruction stencils for edges arranged normally to the body surface are constructed in perfect analogy with the two-dimensional case and their construction does not cause any difficulty, while choosing reconstruction stencils on edges lying on interfaces of prismatic mesh layers is complicated by the absence of mesh structure on these surfaces.

To determine stencils of curvilinear reconstructions in the tangential direction, we propose the following algorithm. At the preprocessing stage, the levels of remoteness of mesh nodes from the body surface are determined by analogy with the two-dimensional case. Following the two-dimensional case, the numerical flux between nodes of different remoteness levels is determined as in the original EBR scheme using rectilinear reconstructions. On the edge ij joining neighboring nodes i and j of the same remoteness level, the variables are reconstructed according to the following algorithm, which is illustrated in Fig. 4:

1. For each of the nodes of edge ij, construct the sets of its first- and second-order neighbor nodes.

2. Exclude from these sets the nodes with remoteness levels different from those of nodes i and j.

3. To each of the constructed sets of nodes, assign the set of mesh edges with both nodes belonging to this set.

4. Specify the projection plane through edge ij by the vector $\mathbf{P}$ that is the half-sum of the normals to the faces incident to edge ij and belonging to the isosurface of the remoteness level of nodes i and j. If there is only one incident face, the vector $\mathbf{P}$ is set equal to the normal to this face. If there are no such faces, then the reconstruction along edge ij is based on the original EBR scheme with rectilinear reconstructions and the subsequent steps of this algorithm are dropped.

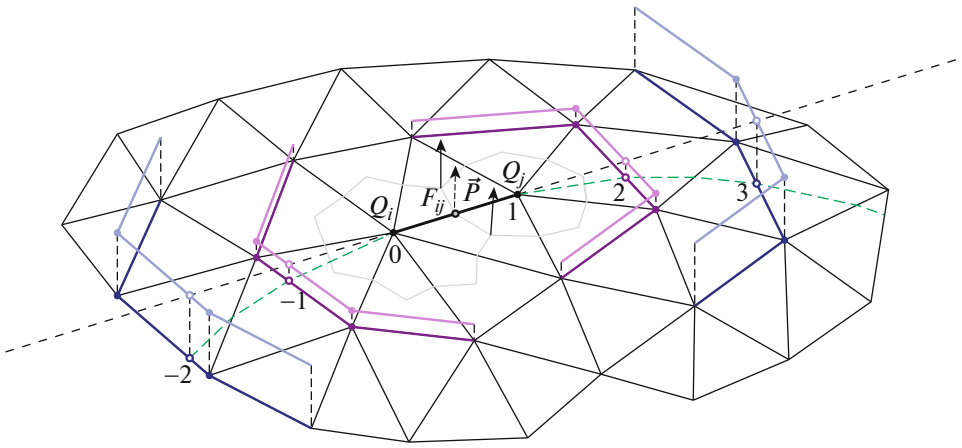

Fig. 4. Algorithm for finding the points of a curvilinear stencil for the reconstruction of variables in the EBR5 SS scheme.

5. Project the sets of edges obtained at Step 3 onto the projection plane specified by the vector **P** and containing edge ij. On this plane, construct a two-dimensional stencil of rectilinear reconstruction by applying the original EBR scheme in the two-dimensional formulation.

6. Determine a curvilinear reconstruction by formulas (2) with metric coefficients corresponding not to the stencil points of rectilinear reconstruction in the projection plane, but rather to their preimages lying on the isosurface of the corresponding remoteness level and thus determining the stencil points of curvilinear reconstruction.

When EBR5 is used as a baseline scheme in semi-structured mesh domains, switching between curvilinear and rectilinear reconstructions in unstructured zones is performed step by step as in the two-dimensional case. In what follows, in the description of numerical results, constructed according to the above-described algorithm, three-dimensional EBR schemes with curvilinear reconstructions in semi-structured domains are denoted as EBR SS (Semi-Structured).

Note that this approach to the construction of curvilinear reconstructions can also be applied to hexahedral layers of structured meshes, but, in this case, it is easier to use the purely structured approach, in which reconstruction stencils are determined along mesh lines for a given ijk-topology.

5. NUMERICAL RESULTS

5.1. Physical Formulation of the Problem

To evaluate the performance of the EBR modifications described in Section 4, the flow over the NACA0012 airfoil [5] was computed in a series of runs. The flow problem is formulated as follows. The NACA0012 airfoil with a unit chord length is placed in a uniform air flow with Mach number $M_\infty = 0.15$ and temperature $T_\infty = 300$ K. The Reynolds number based on the chord length c is $\mathrm{Re}_c = 6\times10^6$. In this work, we considered three angles of attack: 0°, 10°, and 15°.

5.2. Computational Formulation of the Problem

In the computations, the background flow was characterized by a high turbulence intensity, which was achieved by setting the inlet condition $\nu_t/\nu = 1$, where ν_t is the eddy viscosity and ν is the molecular viscosity.

In the two-dimensional formulation, the computational domain was specified as the square $-500 \le x/c,\ y/c \le 500$ with the leading edge of the airfoil placed at the center $(0,0)$ of the square. In the three-dimensional formulation, the computational domain was the rectangular parallelepiped $-500 \le x/c,\ y/c \le 500,\ 0 \le z/c \le 0.25$ with the leading edge of the airfoil lying on the straight line $(0,0,z)$. The no-slip conditions $\mathbf{u} = 0$, $\nu_t = 0$ and adiabaticity were set on the airfoil surface. At the free boundaries $x/c = \pm500$ and $y/c = \pm500$, in the inlet case, all flow parameters are fixed, except for pressure, which is extrapolated; in the outlet case, on the contrary, only pressure is fixed, while the key flow

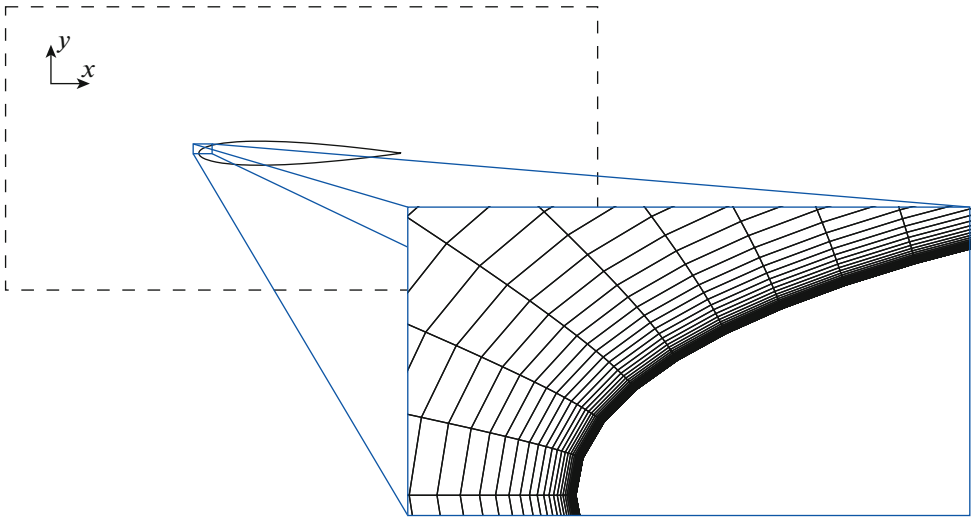

Fig. 5. Mesh configuration.

parameters are extrapolated from the internal domain. In the three-dimensional formulation, periodic conditions were specified at the boundaries $z/c = 0$ and $z/c = 0.25$.

The two-dimensional computations were performed on a sequence of hybrid meshes that were structured trapezoidal near the airfoil and unstructured triangular in the rest of the domain (Fig. 5). The characteristic parameters of these meshes are given in Table 1, where N is the total number of mesh nodes and N_{surf} is the number of nodes on the airfoil surface. In the three-dimensional computations, we used a similar sequence of hybrid meshes which were semi-structured prismatic near the airfoil and unstructured tetrahedral in the rest of the domain. The meshes of this sequence coincided with the corresponding above-indicated two-dimensional meshes at the boundaries $z/c = 0$ and $z/c = 0.25$. The characteristic parameters of the sequence of three-dimensional meshes are given in Table 2, where $N_{\text{surf}, z=0}$ denotes the number of points on the airfoil surface in the plane $z = 0$. Note that x1, ..., x8 are introduced only for notational convenience and are not related to the sequential partition.

In addition to the indicated meshes, for validation computations, we used the two-dimensional structured 897 × 257 mesh that was applied in [5] to obtain reference numerical results. Note that the airfoil geometry on the constructed meshes and the 897 × 257 mesh differed within 1%.

Figure 6 shows the distributions of the dimensionless height y^+ of the first near-wall cell for the airfoil flow incident at angles of attack 0°, 10°, and 15° for two-dimensional meshes. Its counterpart y^+ on three-dimensional meshes has nearly indistinguishable distributions.

The computations were continued until the absolute residual (with respect to the total energy and eddy viscosity) reached a steady state and the lift and drag coefficients reached their asymptotics.

Table 1. Parameters of two-dimensional meshes

2D mesh	x1	x2	x3	x4	x8	897 × 257
N	55 K	51 K	69 K	83 K	84 K	231 K
N_{surf}	102	162	246	442	930	513

Table 2. Parameters of three-dimensional meshes

3D mesh	x1	x2	x3	x4	x8
N	515 K	801 K	1.4 M	2.9 M	9.7 M
N_{surf}	3 K	7 K	15 K	40 K	176 K
$N_{\text{surf}, z=0}$	102	162	246	442	930

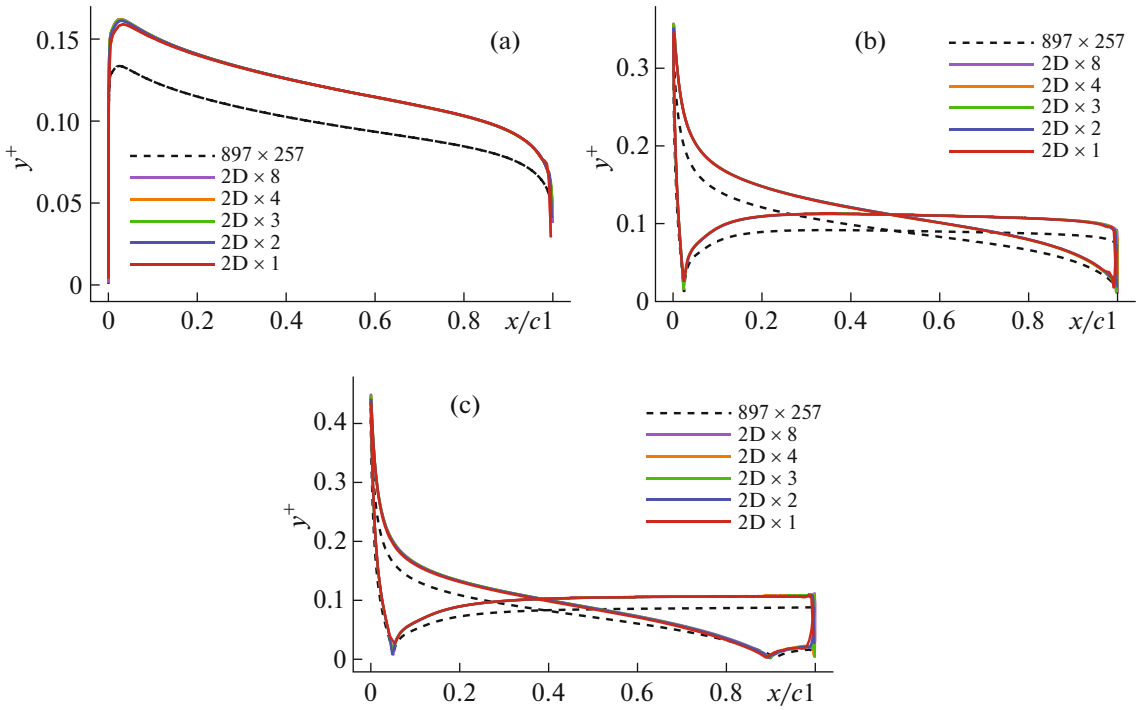

Fig. 6. Dimensionless height y^+ of the first near-wall cell in two-dimensional meshes for the airfoil flow at angles of attack (a) 0°, (b) 10°, and (c) 15°.

5.3. Validation of EBR Schemes with Curvilinear Reconstructions

The EBR IJK and EBR SS schemes were tested on the finest two- and three-dimensional x8 meshes and on the 897 × 257 reference mesh. These schemes and their software implementations were validated by comparing the values of the dimensionless lift (C_l) and drag (C_d) coefficients computed at various angles of attack. Table 3 compares the present numerical results and the data from [5].

Inspection of Table 3 shows that the numerical results produced by existing computer codes differ by 1% for C_l and by 4% for C_d. When they are supplemented with the test results produced by the EBR5 and EBR5 IJK schemes on the 897 × 257 mesh, the difference in C_l remains within 1%, while the discrepancy in C_d increases to 6%. When the initial data are supplemented with the test results produced by the EBR5,

Table 3. Validation results for the EBR5 IJK and EBR5 SS schemes in term of the lift (C_l) and drag (C_d) coefficients

Scheme (mesh)	0°: C_l	10°: C_l	15°: C_l	0°: C_d	10°: C_d	15°: C_d
EBR5 (3D, x8)	~0	1.0862		0.00810	0.01234	
EBR5 SS (3D, x8)	~0	1.0865		0.00810	0.01233	
EBR5 (2D, x8)	~0	1.0875	1.5339	0.00811	0.01239	0.02179
EBR5 IJK (2D, x8)	~0	1.0871	1.5345	0.00812	0.01237	0.02166
EBR5 (897 × 257)	~0	1.0946	1.5437	0.00810	0.01264	0.02219
EBR5 IJK (897 × 257)	~0	1.0940	1.5436	0.00810	0.01259	0.02203
CFL3D (897 × 257)	~0	1.0909	1.5461	0.00819	0.01231	0.02124
FUN3D (897 × 257)	~0	1.0983	1.5547	0.00812	0.01242	0.02159
NTS (897 × 257)	~0	1.0891	1.5461	0.00813	0.01243	0.02105
JOE (897 × 257)	~0	1.0918	1.5490	0.00812	0.01245	0.02148
SUMB (897 × 257)	~0	1.0904	1.5446	0.00813	0.01233	0.02141
TURNS (897 × 257)	~0	1.1000	1.5642	0.00830	0.01230	0.02140
GGNS (897 × 257)	~0	1.0941	1.5576	0.00817	0.01225	0.02073

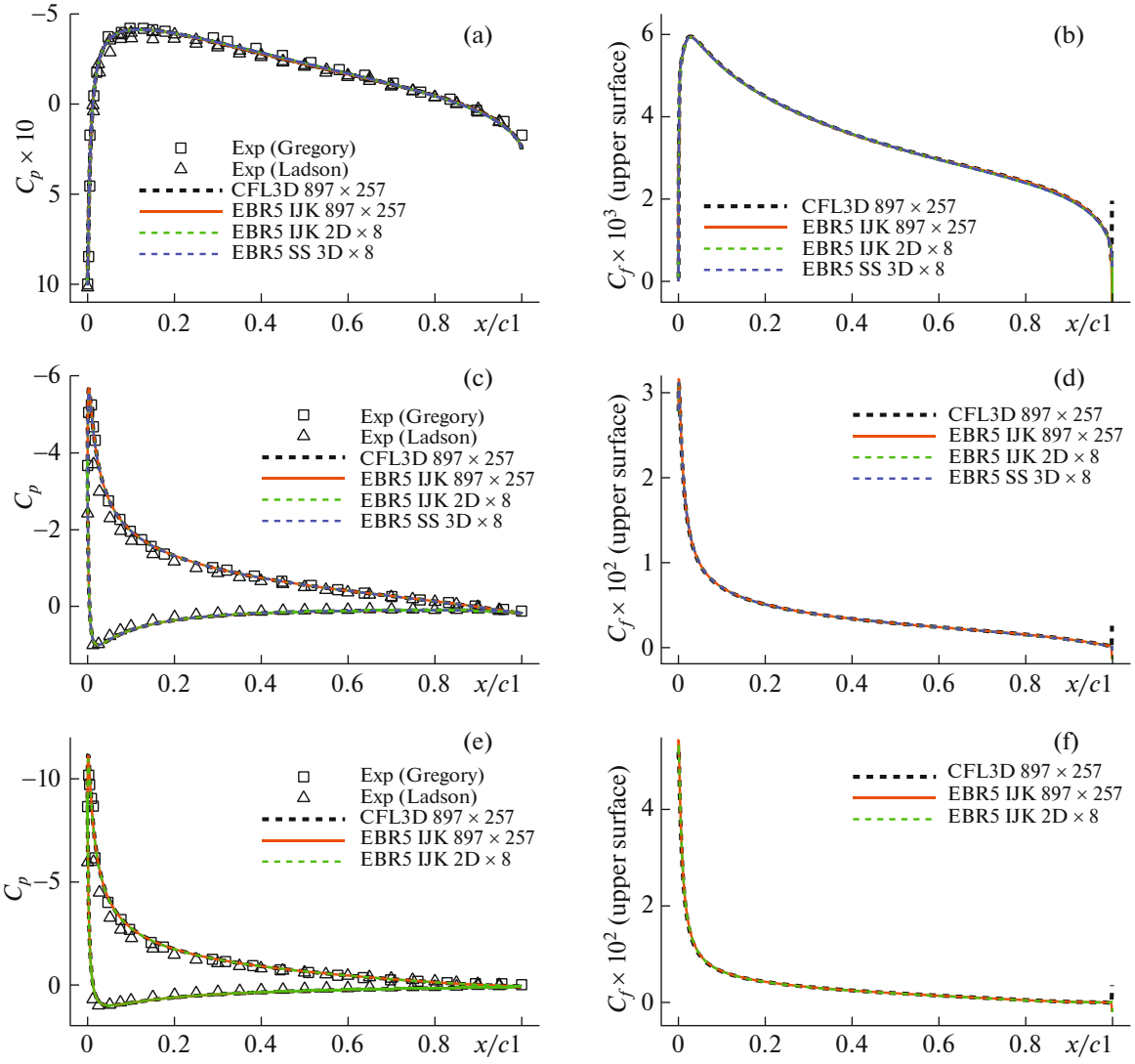

Fig. 7. Validation results for the EBR5 IJK and EBR5 SS schemes: the pressure (C_p) and friction (C_f) coefficients for angles of attack (a), (b) 0°; (c), (d) 10°; and (e), (f) 15°.

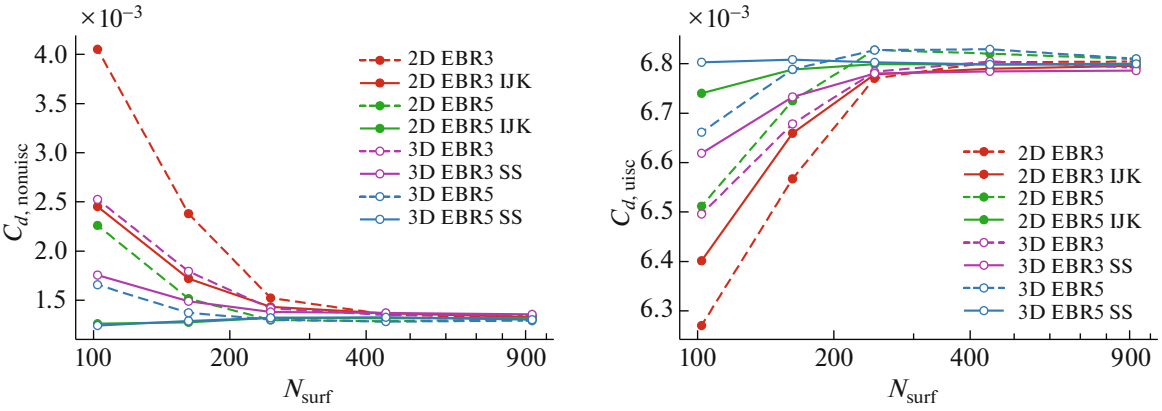

Fig. 8. Inviscid ($C_{d,\text{invisc}}$) and viscous ($C_{d,\text{visc}}$) components of the drag coefficient produced by various schemes on sequences of two- and three-dimensional meshes at zero angle of attack.

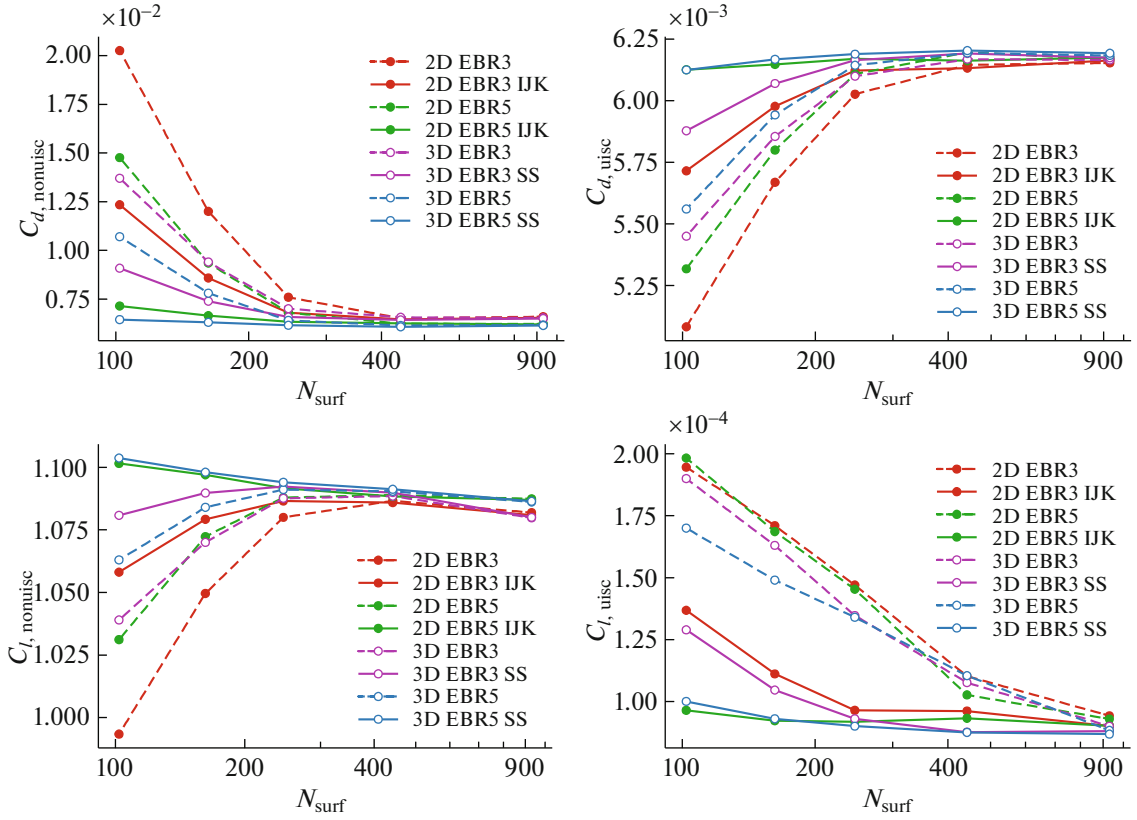

Fig. 9. Components of the drag and lift coefficients produced by various schemes on sequences of two- and three-dimensional meshes at 10° angle of attack.

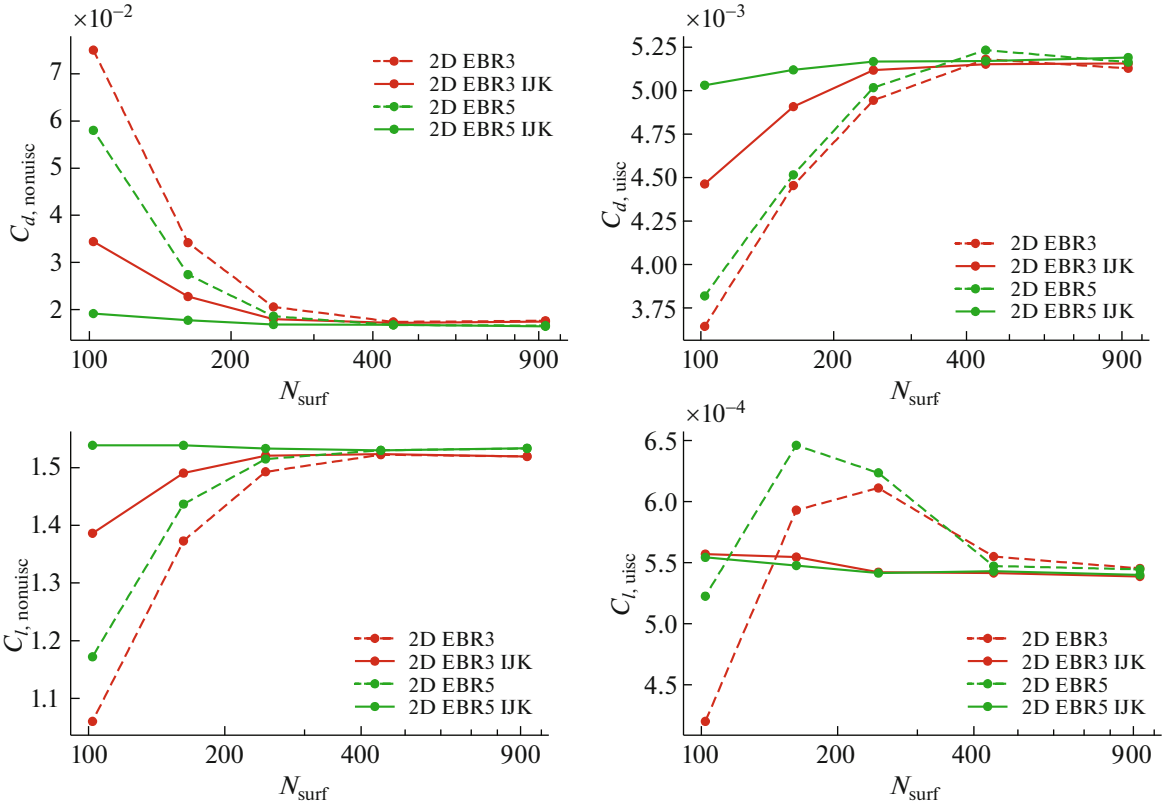

Fig. 10. Components of the drag and lift coefficients produced by various schemes on a sequence of two-dimensional meshes at 15° angle of attack.

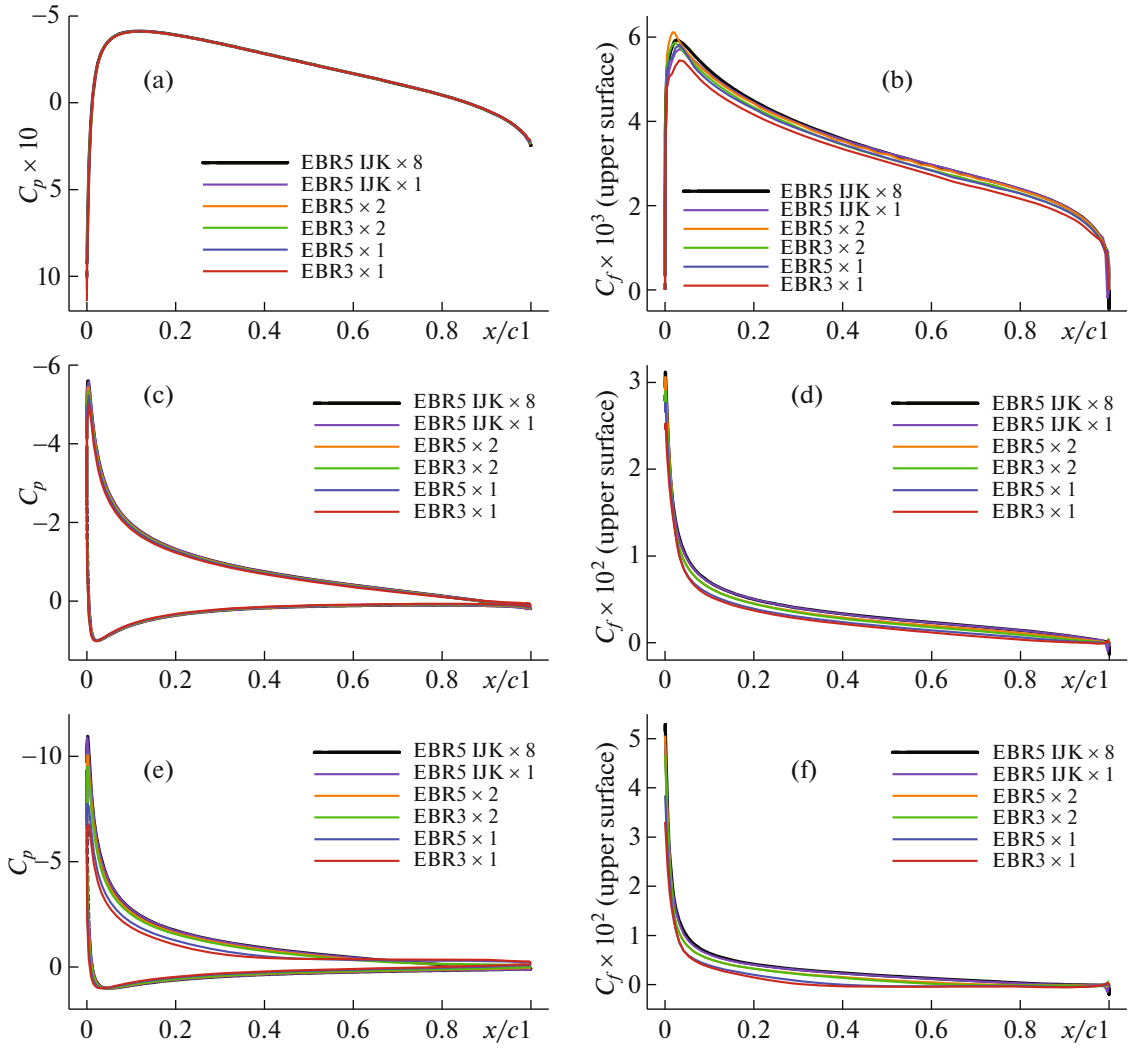

Fig. 11. Most typical distributions of the pressure (C_p) and friction (C_f) coefficients obtained on a sequence of two-dimensional meshes at angles of attack (a), (b) 0°; (c), (d) 10°; and (e), (f) 15°.

EBR5 IJK, and EBR5 SS schemes on two- and three-dimensional x8 meshes, the maximum difference in C_l increases to 2% and the discrepancy in C_d amounts to 5%. For the various types of reconstruction on the same mesh, the difference lies within 0.1% for C_l and within 1% for C_d.

Table 4. Coordinate x/c of the flow separation points for some computations performed on sequences of two- and three-dimensional meshes

Scheme (mesh)	10°	15°
EBR5 IJK (897 × 257)	—	0.91
EBR5 IJK (2D, x8)	—	0.90
EBR5 SS (3D, x8)	—	
EBR5 IJK (2D, x1)	—	0.89
EBR5 2D (2D, x2)	0.994	0.74
EBR3 2D (2D, x2)	0.987	0.66
EBR5 2D (2D, x1)	0.980	0.40
EBR3 2D (2D, x1)	0.935	0.32
EBR5 3D (3D, x1)	—	
EBR3 3D (3D, x1)	0.973	

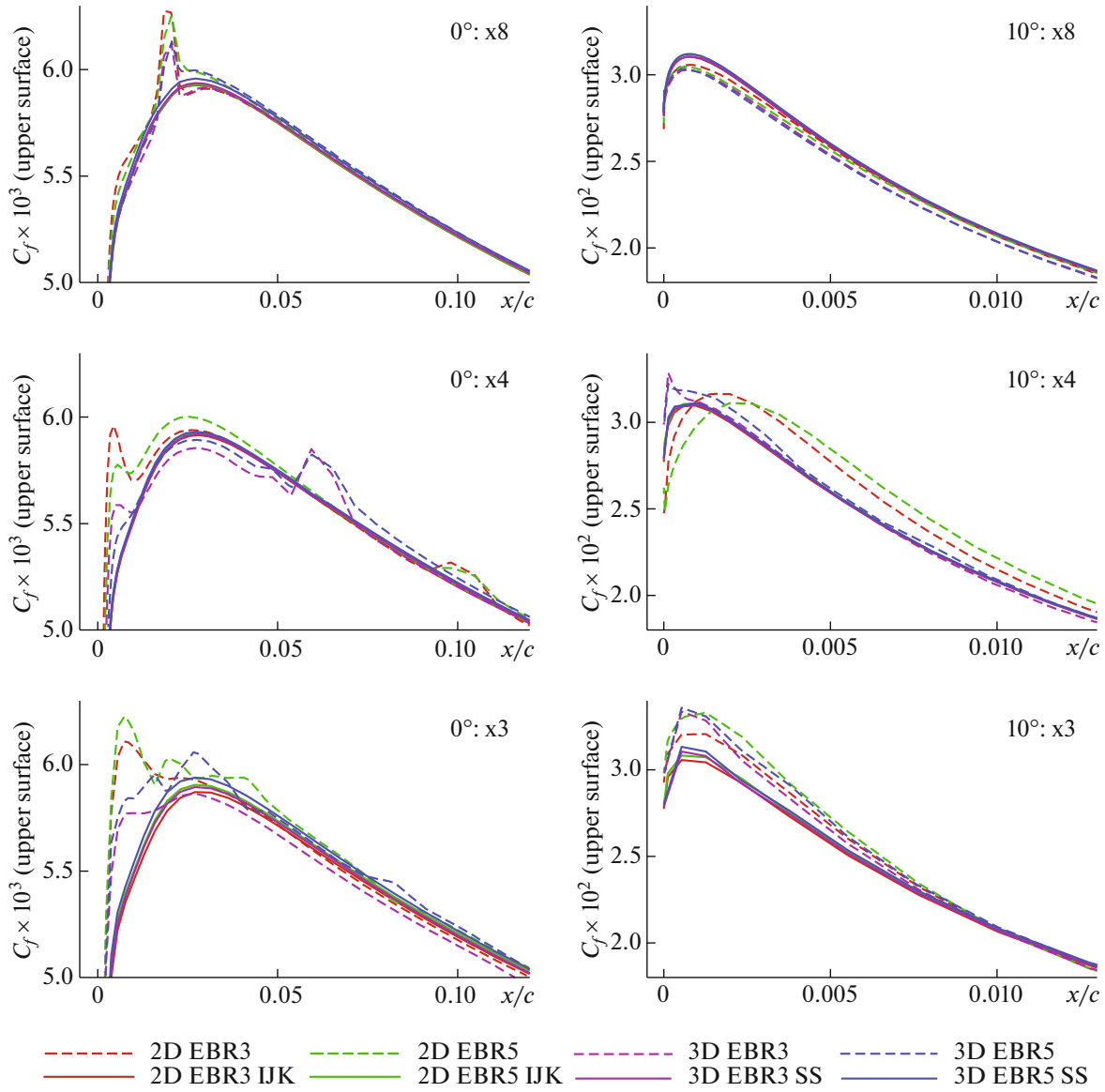

Fig. 12. Friction coefficient distributions in most typical domains obtained on fine meshes at 0° and 10° angles of attack.

In Fig. 7, the numerical distributions of the pressure (C_p) and friction (C_f) coefficients obtained at various angles of attack are compared with the data of [5]. It can be seen that the numerical results agree with the experimental data, and the numerical results for the pressure and friction coefficients produced by different schemes nearly coincide with each other.

Finally, despite the slight increase in the deviations of the integral characteristics from the corresponding reference values and in view of the small differences in the airfoil geometry between the used meshes and the 897 × 257 reference mesh, we can conclude that the numerical results produced by the EBR IJK and EBR SS schemes confirm their applicability to steady aerodynamic flows and the correctness of their software implementation.

5.4. Comparative Analysis of the Results Produced by EBR Schemes with Rectilinear and Curvilinear Reconstructions

Now we consider the numerical results produced by EBR schemes with rectilinear and curvilinear reconstructions on sequences of two- and three-dimensional hybrid unstructured x1, x2, x3, x4, and x8 meshes. As before, the EBR IJK scheme with curvilinear reconstructions was used on two-dimensional

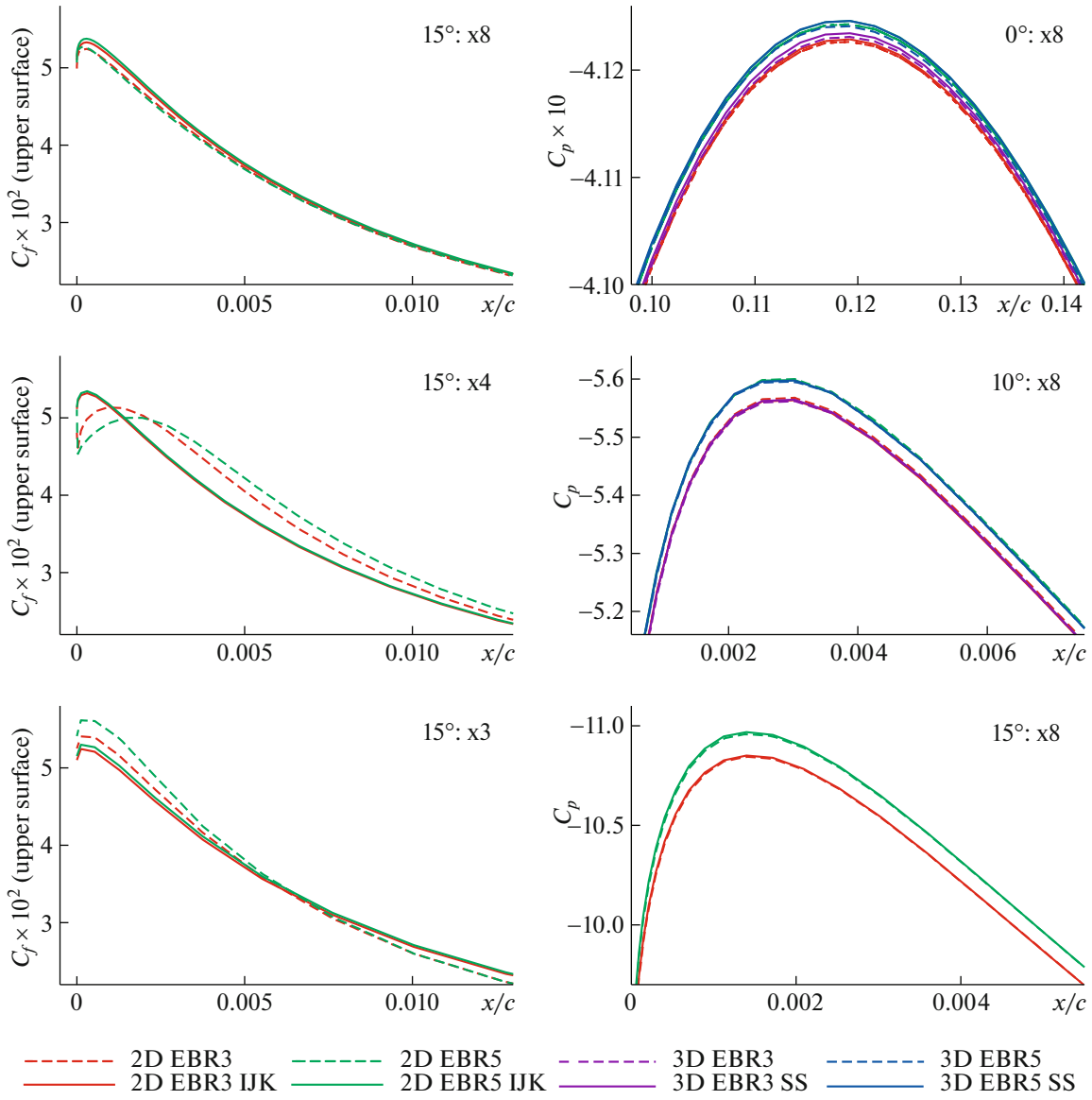

Fig. 13. Friction coefficient distributions in the most typical domain obtained on fine meshes at 15° angle of attack (left), and the pressure coefficient distributions in most typical domains obtained at various angles of attack on x8 meshes (right).

meshes, and the EBR SS scheme with curvilinear reconstructions, on three-dimensional meshes. Note that rectilinear reconstructions on rather coarse x1–x3 meshes often lead to instability issues; its possible causes were discussed above. To ensure the stability of the algorithm in such cases, we introduced a restriction on the maximum admissible ratio of step lengths in the reconstruction stencil and, if it was violated, the algorithm was switched to the EBR3 scheme with the reconstruction coefficient β_{-1} varying, if necessary, as follows. If the value of $|\mathbf{r}_0 - \mathbf{r}_{-1}| \times C_{\text{ratioLim}}$ in formulas (2) was smaller than $|\mathbf{r}_i - \mathbf{r}_j|$, where C_{ratioLim} is a globally specified limiter, then β_{-1} was multiplied by the coefficient $C_{\text{ratioLim}} \times |\mathbf{r}_0 - \mathbf{r}_{-1}| / |\mathbf{r}_i - \mathbf{r}_j|$. For the considered problem and x1–x3 meshes, the value of C_{ratioLim} equal to 20 was found sufficient.

We begin our analysis of the resulting integral characteristics with zero angle of attack (Fig. 8). The results show that, as expected, all the schemes produce less accurate solutions on coarser meshes and better results are obtained on three-dimensional meshes than on similar two-dimensional ones.

On coarse x1–x3 meshes, as expected, the EBR5 scheme and its versions with curvilinear reconstructions demonstrate higher accuracy than the corresponding algorithms based on the EBR3 scheme. More-

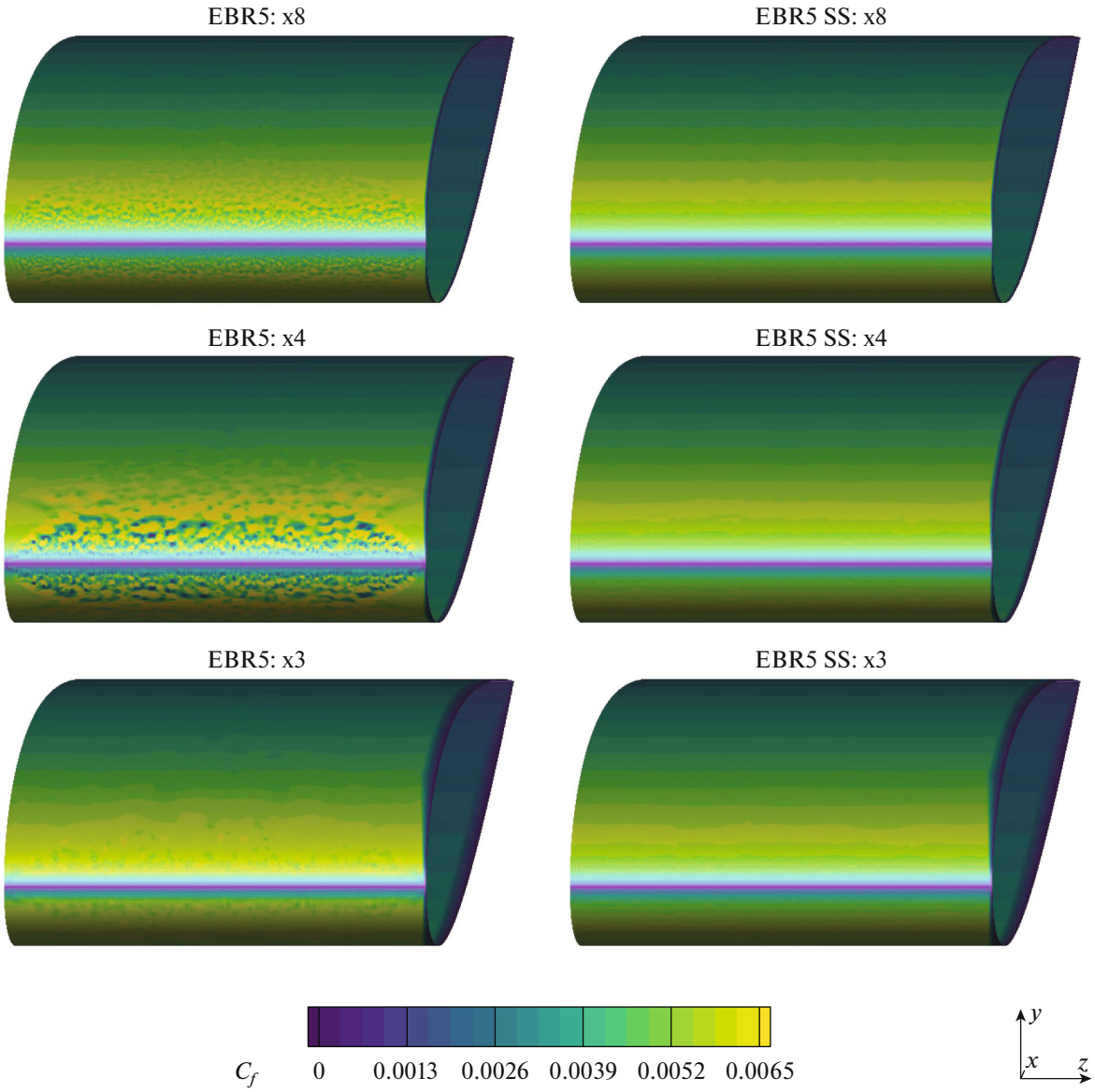

Fig. 14. Friction coefficient distributions over the airfoil surface produced by the EBR5 and EBR5 SS schemes on three-dimensional x8, x4, and x3 meshes at zero angle of attack.

over, the use of curvilinear reconstructions leads to a significant decrease in the error, so that the examined control values obtained in this case even on rather coarse x1 meshes (in both two and three dimensions) become fairly close to the true values obtained on the reference meshes. Additionally, it should be noted that, with an increase in the mesh resolution, the difference between the results produced by the schemes with rectilinear and curvilinear reconstructions is reduced, which is explained by the gradual straightening of the curvilinear reconstruction stencils in the boundary layer under mesh refinement.

The above-drawn conclusions are confirmed by similar results obtained for 10° and 15° angles of attack (Figs. 9 and 10). It should be noted that, at nonzero angles of attack on coarse meshes, the EBR3 scheme, which has a shorter curvilinear stencil, demonstrates higher accuracy than the EBR5 scheme, which involves a more extended, but rectilinear stencil.

To illustrate the performance of the considered EBR schemes on various two-dimensional meshes, Fig. 11 presents typical distributions of the pressure and friction coefficients over the airfoil surface. Inspection of the plots suggests that, for all angles of attack, the largest deviations from the reference numerical results are observed (in decreasing order) for EBR3 on the x1 mesh, EBR5 on the same mesh,

EBR3 on the x2 mesh, EBR5 on the x2 mesh, and EBR5 IJK on the x1 mesh. This sequence is confirmed by the data presented in Figs. 8–10. Once again, we note that the pressure and friction coefficients produced by the EBR5 IJK scheme with curvilinear reconstructions even on the coarsest x1 mesh agree fairly well with the reference results obtained on the finest x8 mesh.

The friction coefficient distributions displayed in Fig. 11 can be used to estimate the variations in the sizes of the recirculation zone. The corresponding coordinates of the separation point are given in Table 4. Inspection of the table reveals that, without using curvilinear reconstructions in the EBR schemes on coarse meshes, the resulting size of the recirculation zone can differ substantially from the corresponding physically correct result. This is especially noticeable for 15° angle of attack. Note also that the use of rectilinear reconstructions on coarse meshes might lead to false separation, which can be observed at 10° angle of attack.

Curvilinear reconstruction are beneficial not only on coarse, but also on rather fine meshes. This can be seen by analyzing the friction coefficient distributions presented in Figs. 12 and 13. First, for schemes with rectilinear reconstructions in both two- and three-dimensional cases, the friction coefficient converges to the reference value much more slowly and less regularly than for similar schemes with curvilinear reconstructions. Second, despite the overall convergence, there might be areas where the differences from the reference values remain considerable, which is especially pronounced at zero angle of attack.

Figure 13 presents the pressure coefficient distributions in the most typical domains obtained on the finest x8 meshes for various angles of attack.

Figure 14 shows the friction coefficient distributions over the airfoil surface for three-dimensional flow at zero angle of attack produced by the EBR5 schemes on fine meshes. It can be seen that the rectilinear reconstructions give rise to spurious oscillations, while the curvilinear reconstruction allow us to avoid this effect. A similar situation is observed for EBR3 schemes and nonzero angles of attack.

The conducted analysis suggests that the proposed generalizations of EBR schemes to curvilinear reconstruction stencils in structured or semi-structured mesh domains not only work correctly, but are also highly desirable on anisotropic meshes in boundary-layer domains, which are used in the simulation of turbulent flows at high Reynolds numbers.

All the computations described in this paper were performed using the NOISEtte code [14].

CONCLUSIONS

EBR schemes on hybrid unstructured meshes were generalized by supplementing them with the option of performing edge-based reconstructions not along the straight line containing this edge, but rather along the curve containing it. The implementation of this option provides a number of important advantages for the simulation of flows around bodies of arbitrary geometry.

First, reconstructions based on a curvilinear stencil in structured and semi-structured mesh domains in the near-wall region make it possible to obtain higher accurate numerical solutions due to the better alignment of the stencil with the flow.

Second, curvilinear reconstructions make it possible to avoid sharp variations in the distances between stencil nodes, which usually arise in the original EBR schemes due to the intersection of rectilinear reconstruction of the layered mesh structure with anisotropic elements. The strong nonuniformity of the stencil steps and the large variations in the values of variables at its nodes, which arise when the points of a rectilinear stencil belong to different boundary-layer regions, substantially reduce the accuracy of the approximation and degrade the stability of the numerical method. These difficulties can be overcome by introducing curvilinear stencils and curvilinear reconstructions on them.

The proposed implementation of curvilinear reconstructions does not increase the computational cost of the numerical algorithm and does not reduce its parallel efficiency as compared with the original EBR scheme using rectilinear reconstructions.

The simulation of the turbulent flow over the NACA0012 airfoil was used to demonstrate the advantages of applying curvilinear reconstructions, which consist in more stable computations and more accurate and acceptable (from an engineering point of view) results obtained even on rather coarse meshes.

ACKNOWLEDGMENTS

We are grateful to our colleague P.A. Bakhvalov for valuable comments and helpful discussions.

FUNDING

This work was supported by the Russian Foundation for Basic Research (project no. 18-01-00445). Computing resources were provided by the Shared Facility Center of the Keldysh Institute of Applied Mathematics of the Russian Academy of Sciences and by the Center for collective use of high-performance computing resources at Lomonosov Moscow State University.

REFERENCES

1. I. V. Abalakin, P. A. Bakhvalov, and T. K. Kozubskaya, "Edge-based reconstruction schemes for unstructured tetrahedral meshes," Int. J. Numer. Methods Fluids **81** (6), 331–356 (2016).
2. P. A. Bakhvalov and T. K. Kozubskaya, "On efficient vertex-centered schemes on hybrid unstructured meshes," AIAA Paper 2016–2966, *22nd AIAA/CEAS Aeroacoustics Conference* (2016).
3. A. J. Katz and D. Work, "High-order flux correction/finite difference schemes for strand grids," J. Comput. Phys. **282**, 360–380 (2015).
4. O. Tong, A. J. Katz, A. M. Wissink, and J. Sitaraman, "High-order methods for three-dimensional strand-Cartesian grids," AIAA Paper 2015–0835, *53rd AIAA Aerospace Sciences Meeting* (2015).
5. NASA Langley Research Center. Turbulence Modeling Resource. 2DN00: 2D NACA 0012 Airfoil Validation Case. https://turbmodels.larc.nasa.gov/naca0012_val.html. SA Model Results https://turbmodels.larc.nasa.gov/naca0012_val_sa.html
6. P. R. Spalart and S. R. Allmaras, "A one-equation turbulence model for aerodynamic flows," AIAA Paper 92–0439, *30th Aerospace Science Meeting* (1992).
7. P. A. Bakhvalov and T. K. Kozubskaya, "EBR-WENO scheme for solving gas dynamics problems with discontinuities on unstructured meshes," Comput. Fluids **157**, 312–324 (2017).
8. P. A. Bakhvalov, Preprint No. 79, IPM RAN (Keldysh Inst. of Applied Mathematics, Russian Academy of Sciences, Moscow, 2017).
9. A. P. Duben and T. K. Kozubskaya, "On scale-resolving simulation of turbulent flows using higher-accuracy quasi-1D schemes on unstructured meshes," Progress in Hybrid RANS-LES Modelling. HRLM (2016). Notes Numer. Fluid Mech. Multidiscip. Design **137**, 169–178 (2016).
10. Y. Kallinderis and S. Ward, "Prismatic grid generation for three-dimensional complex geometries," AIAA J. **31** (10), 1850–1856 (1993).
11. S. Connell and M. Braaten, "Semi-structured mesh generation for 3D Navier–Stokes calculations," AIAA Paper 92–0439, *12th Computational Fluid Dynamics Conference* (1995).
12. A. Khawaja and Y. Kallinderis, "Hybrid grid generation for turbomachinery and aerospace applications," Int. J. Numer. Methods Eng. **49** (1–2), 145–166 (2000).
13. A. N. Athanasiadis and H. Deconinck, "A folding/unfolding algorithm for the construction of semi-structured layers in hybrid grid generation," Comput. Methods Appl. Mech. Eng. **194** (48–49), 5051–5067 (2005).
14. A. Gorobets, "Parallel algorithm of the NOISEtte code for CFD and CAA simulations," Lobachevskii J. Math. **39** (4), 524–532 (2018).

Translated by I. Ruzanova